Preparation and microstructure characterization of iron oxide pellets for hydrogen storage

Karel Soukup, Jan Rogut, Jacek Grabowski, Marian Wiatowski, Magdalena Ludwik-Pardała, Petr Schneider, and Olga Šolcová

***Abstract*—**The redox cycle of iron oxides ($Fe_3O_4 + 4H_2 \leftrightarrow 3Fe + 4H_2O$) which can be applied as a new method of storage and supply of hydrogen were studied. The iron oxides were prepared by precipitation of aqueous ferric nitrate. The addition of aluminium oxide into iron oxides prevented the sintering of metal iron and/or iron oxides during repeated redox cycles. The optimal calcination temperature for cylindrical pellets preparation was found to be 850 ^oC. Transport parameters for Fe_2O_3/Al_2O_3 and Fe/Al_2O_3 samples, which can be utilized for optimization of porous structure for hydrogen storage, were determined by the chromatographic technique in the single pellet-string arrangement.

***Keywords*—**Hydrogen storage, Steam iron process, Transport parameters, Inverse gas chromatography.

I. Introduction

Hydrogen storage is one of the hydrogen economy problems because of the lack of safe, efficient and low cost storage methods. Especially in on-board applications (e.g. hydrogen based fuel-cell vehicles) the storage of hydrogen is a key issue. So far, three main ways are used: liquefaction, compression and the use of solid sorbents (carbon nanotubes, activated carbon, fullerenes, absorbing alloys and metal hydrides based on Mg, Na, Li, B, etc. [1]). These methods has several weak points: liquefaction is economically very demanding because it requires a huge amount of energy as well as developments of high-efficiency technologies in the hydrogen liquefaction processes, the design of cryogenic hydrogen tanks and the safe handling systems for loading and unloading liquid hydrogen. A serious safety problem is connected with hydrogen compression; and solid adsorbents can adsorb generally only a small amount of hydrogen. Hydrogen-absorbing alloys are generally sensitive to oxygen and water and usually require high pressures (>10 bar) for the absorption of hydrogen.

There exists another, long known approach for hydrogen storage based on the steam iron process [2], which has been intensively studied at the beginning of the 20th Century. By this method, hydrogen storage can be described as a reduction of iron oxides to metallic iron by hydrogen [3]–[8] according following equation:

$$Fe_3O_4 + 4H_2 \rightarrow 3Fe + 4H_2O \quad (1)$$

and hydrogen production is achieved through the oxidation of iron by steam water according to

$$3Fe + 4H_2O \rightarrow Fe_3O_4 + 4H_2 \quad (2)$$

In this method hydrogen is not stored directly, because redox cycle of iron/iron oxides works apparently as a medium for hydrogen storage. Theoretical amount of hydrogen stored as Fe metal is 4.8 wt. %. At high temperature and pressure the reaction equilibrium is shifted to the right (i.e. hydrogen storage), at lower temperature and pressure the equilibrium is shifted to the left (i.e. hydrogen recovery) [8]. High repeatability of these cycles can be achieved by addition of various additives (e.g. Al_2O_3) to iron [9], [10]. The iron and iron oxide are cheap and environmental-friendly materials. These materials are stable under atmosphere at room temperature, thus easy to be handled [11]. Furthermore, since the fuel is just water, there is no risk of explosion when the vehicles collide. The very clean produced hydrogen (no CO traces) is suitable for fuel cells.

Fe_2O_3 is a precursor from which iron and Fe_3O_4 is obtained. Therefore, we have tried to prepare porous pellets of Fe_2O_3 and Fe with the use of Al_2O_3 (α-alumina) as an additive and studied their textural and transport characteristics. The aim of this study is acquisition of information on pellets texture from the nitrogen physical adsorption isotherms and mercury porosimetry, true pellets densities followed from helium pycnometry as well the pellet transport characteristics

Manuscript received December 30, 2010. The financial support of European Commission Research Program of the Research Fund for Coal and Steel (RFCR-CT-2007-00006) and Ministry of Education, Youth and Sports of the Czech Republic (7C08033) is gratefully acknowledged.

K. Soukup is with the Institute of Chemical Process Fundamentals of the ASCR, v.v.i., Rozvojová 135, CZ-165 02 Praha 6, Czech Republic (corresponding author to provide phone: +420 220 390 282; fax: +420 220 920 661; e-mail: soukup@icpf.cas.cz).

J. Rogut is with Central Mining Institute, Plac Gwarków 1, 40-166 Katowice, Poland (e-mail: rogutjan@yahoo.com).

J. Grabowski is with Central Mining Institute, Plac Gwarków 1, 40-166 Katowice, Poland (e-mail: sixjg@gig.katowice.pl).

M. Wiatowski is with Central Mining Institute, Plac Gwarków 1, 40-166 Katowice, Poland (e-mail: mwiatowski@gig.eu).

M. Ludwik-Pardała is with Central Mining Institute, Plac Gwarków 1, 40-166 Katowice, Poland (e-mail: mludwik@gig.katowice.pl).

P. Schneider is with the Institute of Chemical Process Fundamentals of the ASCR, v.v.i., Rozvojová 135, CZ-165 02 Praha 6, Czech Republic (e-mail: schneider@icpf.cas.cz).

O. Šolcová is with the Institute of Chemical Process Fundamentals of the ASCR, v.v.i., Rozvojová 135, CZ-165 02 Praha 6, Czech Republic (e-mail: solcova@icpf.cas.cz).

evaluated by the inverse gas chromatography method in the single pellet-string column arrangement (SPSC) [12]

II. Experimental

A. Preparation of Fe_2O_3/Al_2O_3 composite powders

Composite Fe_2O_3/Al_2O_3 samples with 1:1 Fe/Al molar ratio were prepared as follows: first, the Al_2O_3 sample (POCh Gliwice, Poland) was grinded in the agate mill for 3 hours to obtain fine alumina powder. In a typical case 404 g of $Fe(NO_3)_3.9H_2O$ was dissolved in hot demineralised water and 51 g of Al_2O_3 fine powder was mixed for approximately 10 minutes in 200 ml hot demineralised water. Then, the solution of $Fe(NO_3)$ was added into the mixed Al_2O_3 suspension and 225 g of 25 % ammonia was continuously poured with the rate 1 cm^3/s. The $Fe(OH)_3$ precipitation process on the Al_2O_3 support was carried out according to the equation:

$$Fe(NO_3)_3 + 3\ NH_4OH \rightarrow Fe(OH)_3 + 3\ NH_4NO_3 \quad (3)$$

The prepared solution was gelated slowly and thereafter the product was mixed for 10 minutes. The obtained solution was drained off in a Buchner funnel for 5 hours; the resulted sediment was washed with water and afterwards dried at 150 °C. The brown hydrated particles of contaminated $Fe(OH)_3$ were grounded in the quern mill and calcined in a muffle furnace at 1000 °C until the brown smoke of NO_x disappeared. The powder was cooled to ambient temperature and washed with 5 l of water, dried and calcined at 1000 °C again. The composite was grounded in the agate mill after cooling and then sieved to fraction with grains diameter below 0.063 mm. The larger grains were grounded again. 82 g of Fe_2O_3/Al_2O_3 powder was prepared by this technique.

The SEM photo of prepared Fe_2O_3/Al_2O_3 particles is shown in Fig. 1. Black clusters represent ferric oxide. The white clusters correspond to alumina. From Fig. 1 a good homogeneity of the prepared mixture of Fe_2O_3/Al_2O_3 can be recognized.

B. Preparation of cylindrical pellets Fe_2O_3/Al_2O_3

Mechanically stable cylindrical pellets of Fe_2O_3/Al_2O_3 (5 x 5 mm = diameter x height) were prepared from powdered mixture of aluminium oxide and ferric oxide. 77.55 g of the powdered sample was mixed with 11.08 g binder (based on a form of silica: Glazura Pw 137, Glazura s.r.o., Czech Republic). Water suspension was prepared by adding 71 ml of distilled water; the water suspension was thoroughly stirred for

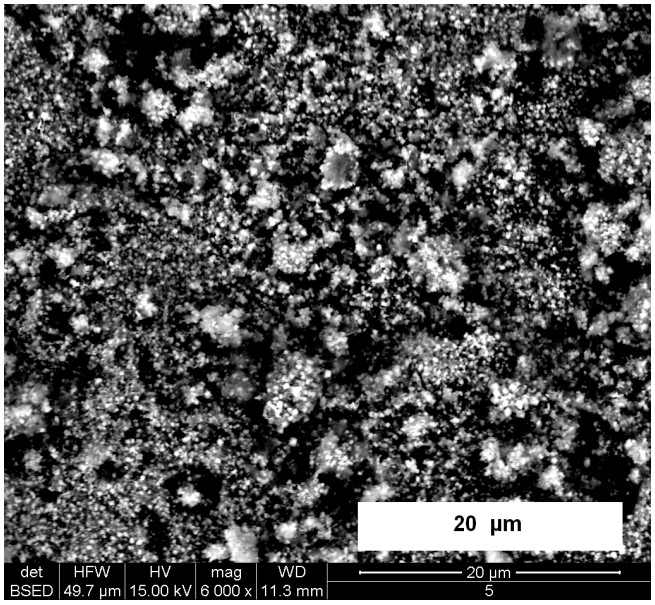

Fig. 1 SEM image of prepared Fe_2O_3/Al_2O_3 powders

approximately 90 min and poured into 124 cylindrical holes (5 x 5 mm height/diameter) drilled into a stable plastic disc with a syringe. Pellets were then manually pressed out of the holes using a metallic piston. The pellets were dried by evaporation overnight at room temperature and finally, calcined with temperature gradient 2 °C/min in air at 550 °C (denoted as Sample 1), 700 °C (Sample 2), 850 °C (Sample 3) and 950 °C (Sample 4) for 10 minutes. The total number of prepared porous pellets was approximately 350.

C. Preparation of Fe/Al_2O_3 pellets

Fe_2O_3/Al_2O_3 pellets calcined at 850 °C (Sample 3) were reduced at 800 °C for one hour by hydrogen, which was sufficient for complete reduction of Fe_2O_3, see XRD patterns in Figs. 5 and 6.

D. Pellets characterization

The structure of prepared powder samples Fe_2O_3/Al_2O_3 and Fe/Al_2O_3 was studied by X-ray diffraction. X-ray powder diffraction data were collected at room temperature with an X'Pert PRO θ-θ powder diffractometer (PANalytical B.V., the Netherlands) with parafocusing Bragg-Brentano geometry using CuK_α radiation (with basic parameters: $\lambda = 1.5418$ Å, U = 40 kV, I = 30 mA).

For high-pressure mercury porosimetry the porosimeter AutoPore III was used. Nitrogen adsorption isotherms were obtained with ASAP 2020. True (helium) density was determined with the AccuPyc 1330. All instruments are from Micromeritics, USA.

Textural properties are summarized in Table I, where T_c denotes calcination temperature, S_{BET} stands for the internal surface area determined from the classic BET isotherm, V_{micro} is the micropore volume obtained from the modified (three parametric) BET isotherm and finally, ε denotes the porosity calculated from the apparent density and the true density as

TABLE I
TEXTURAL PROPERTIES OF Fe_2O_3/Al_2O_3 CYLINDRICAL PELLETS

Sample	T_c	S_{BET}	V_{micro}*	ε	Mechanical stability
	[°C]	[m²/g]	[mm³/g]	[–]	
1	550	6.7	1.7	0.46	–
2	700	18.2	4.3	0.66	+
3	850	17.5	4.2	0.66	++
4	950	0.4	0.7	0.08	+++

* volume of micropore

$\varepsilon = 1 - \rho_{Hg} / \rho_{He}$.

Pore-size distributions for the samples calcined at various temperatures obtained by mercury porosimetry are depicted on Fig. 2.

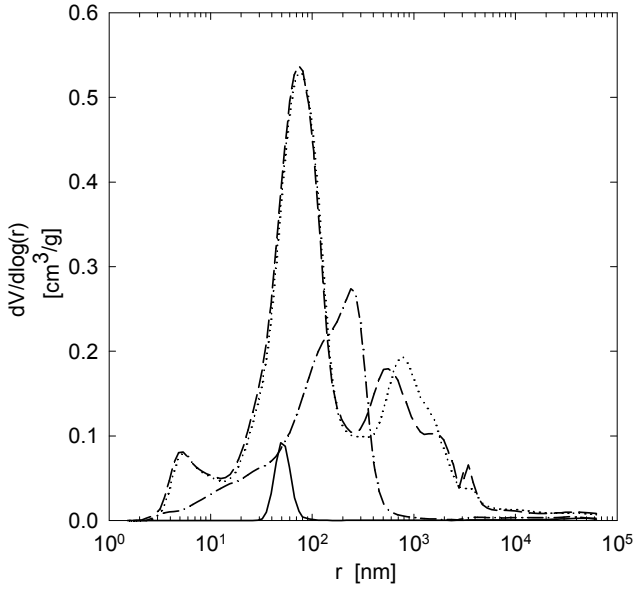

Fig. 2 Pore-size distribution curves for all tested samples. (– . – . –): Sample 1 (calc. 550 °C); (– – –): Sample 2 (calc. 700 °C); (.....): Sample 3 (calc. 850 °C); (—): Sample 4 (calc. 950 °C)

E. Chromatographic setup

The inverse gas chromatography setup (see Fig. 3) consists of a chromatographic column, a thermal conductivity detector (Micro-TCD 10-955, Gow-Mac Instruments Co., USA), calibrated mass flow-meters/controllers (Brooks 5850S, Brooks Instruments, the Netherlands), six port sampling valve (sample volume 250 µl) with an electric actuator (Valco Instruments Co. Inc., USA). Two columns with lengths 100 cm and 50 cm and identical inner diameter (0.67 cm) were packed either with ferric oxide (Fe_2O_3/Al_2O_3) or reduced (Fe/Al_2O_3) pellets. All chromatographic measurements were performed at laboratory temperature and pressure. Argon, nitrogen and helium were selected both as carrier and tracer gases. Five different carrier gas flow rates were used: 30, 60, 90, 150 and 250 cm³/min.

Approximately 3000 response points from the TCD detector were recorded on a digital data logger. After zero-line correction (less than 0.1 % of the maximum response height) about 90 uniformly distributed experimental points were normalized to the maximum of the tracer concentration. The final response signals were obtained by averaging three individual peaks for each carrier gas flow rate and carrier/tracer pair of gases. The transport characteristics were evaluated from averaged response signals.

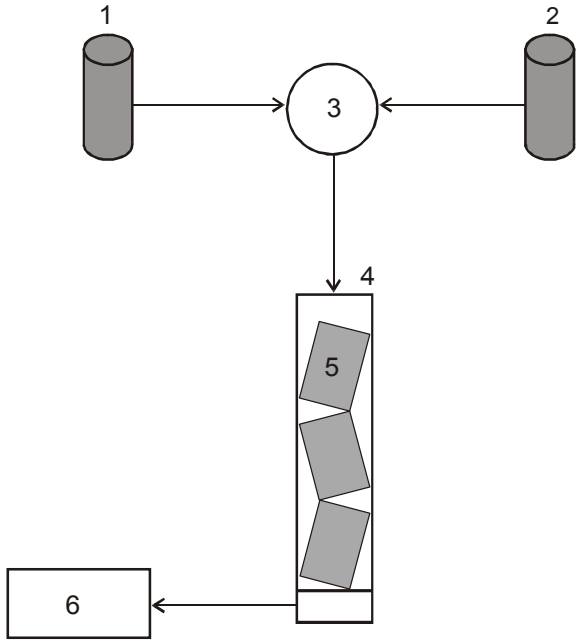

Fig. 3 Inverse gas chromatography setup. (1): carrier gas source; (2): tracer gas source; (3): six-way sampling valve; (4): chromatographic column; (5): tested cylindrical samples; (6): PC with digital data logger

F. Chromatographic data evaluation

Transport parameters were evaluated from response (chromatographic) signals of columns packed with particles of the tested porous material. A pulse of tracer gas (T) is injected into the carrier-gas (C) stream, which flows at constant flow rate through the column. The tracer concentration is measured at the column outlet by a detector. The recorded outlet response signal was then analyzed. Analysis of outlet peaks was based on the transport processes inside the column. The transport model by Kubín-Kučera [13], [14] has been usually used. Matching of column response peaks with model equations was usually done via the response moments [15].

Nowadays, it is possible to perform the matching in the time domain [16]. The Kubín-Kučera model describes intracolumn processes, such as convection and axial dispersion of the tracer band, transport of the tracer through a laminar film around the packing particles, diffusion in the pore structure and adsorption (for adsorbable tracer gas) on the internal surface of porous packing as well extra-column effects account for processes upstream and downstream of the colum. It has been suggested [17] that these processes can be included in the

time-domain matching through application of the convolution theorem.

For the tracer/carrier gas system the impulse response of the column packed with porous spherical particles of radius R, in which tracer equilibrium adsorption in the Henry region of the adsorption isotherm and intraparticle diffusion characterized by the effective diffusion coefficient, D_{TC}, is given by equation [16]:

$$h(t) = Q\int_0^\infty \exp\left(\frac{Pe}{2} - f_1\right)\cos\left(\frac{2\lambda^2 t}{t_{dif}} - f_2\right)\lambda \mathrm{d}\lambda \tag{3}$$

where:

$$f_{1,2} = \sqrt{\frac{\sqrt{A^2 + B^2} \pm A}{2}}$$
$$A = Pe\left(\frac{Pe}{4} + \frac{3\gamma H_1 t_c}{t_{dif}}\right)$$
$$B = Pe\frac{t_c}{t_{dif}}\left(\frac{2\gamma\lambda^2}{\delta_0} + 3\gamma H_2\right) \tag{4}$$
$$H_1 = \lambda\frac{\sinh(2\lambda) + \sin(2\lambda)}{\cosh(2\lambda) - \cos(2\gamma)} - 1$$
$$H_2 = \lambda\frac{\sinh(2\lambda) - \sin(2\lambda)}{\cosh(2\lambda) - \cos(2\gamma)}$$

and t_c is the tracer mean residence time in the column of length L ($t_c = L/v$) with carrier gas linear velocity, v. Pe is the Peclet number ($Pe = vL/E_{TC}$ with the axial dispersion coefficient, E_{TC}), t_{dif} denotes the diffusion time of the tracer in the pore structure of the pellet, $t_{dif} = R^2\beta/D_{TC}$, where R denotes the radius of the pellet equivalent sphere, δ_0 id the tracer adsorption parameter, $\delta_0 = \gamma(1 + K_T)$, with $\gamma = \beta(1 - \alpha)/\alpha$. β is the pellet porosity and α is the column void fraction (interstitial void volume/column volume). Thus, γ, is the pore volume per unit interstitial volume. For an inert tracer $K_T = 0$ and thus $\delta_0 = \gamma$. Q in (3) is a normalization constant defined so that the calculated response maximum the tracer concentration equals unity, $c(t_{max}) = 1$.

G. Extra column effects elimination

Equations (3) and (4) describe correctly the intracolumn processes but neglect the effects of processes upstream and downstream of the column (extra column effects, ECE). In the time-domain fitting it is possible to include these effects through the application of the convolution theorem [17]. This requires, besides the knowledge of the experimental system response, also the knowledge of the ECE response. The ECE can be replaced by experimental system responses for two columns with different length. The convolution theorem states that the column response, $c(t)$, is given by the convolution integral [17]:

$$c(t) = \int_0^t g(t-u)h(u)\mathrm{d}u \tag{5}$$

where $h(t)$ represents the column impulse response and $g(t)$ describes the shape of the signal entering the column instead of the Dirac impulse. In linear systems it is immaterial of the ECE are distributed in different places of the system or if they are concentrated in one place and in what order they are arranged. Therefore, it is possible to use the experimental responses for the shorter column as $g(t)$.

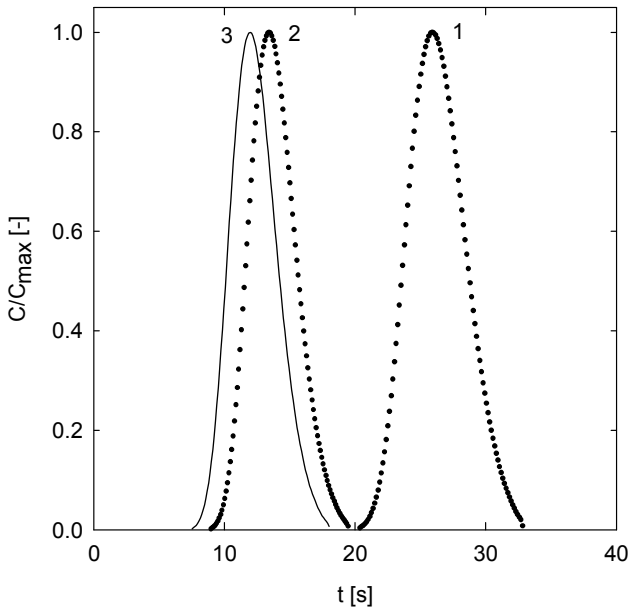

Fig. 4 Experimental response signals for columns of length 100 cm (1), 50 cm (2) and the calculated impulse response (3) for lengths 50 cm

Fig. 4 shows the experimental response signals for column lengths 100 cm (1) and 50 cm (2). All peaks were normalized to the same height. Peak 3 is the calculated response for a column length 100 – 50 = 50 cm when extra-column effects are eliminated via the convolution integral and correspond to a true impulse response. Because the length of longer column is double of the length of shorter column, the difference between peaks 2 and 3 belongs to extra column effects.

H. Model of porous solids

As a model of the pore structure the mean transport pore model (MTPM) [18] has been used, which assumes that the decisive part of the gas transport takes place in transport pores that are visualized as cylindrical capillaries with radii distributed around the mean value $\langle r \rangle$ (first model parameter). The ratio of porosity, ε_t, to tortuosity of transport pores, q_t, $\psi = \varepsilon_t/q_t$ is the second model parameter. Transport parameters represent material properties of the porous solid, and thus do not depend on temperature, pressure or the kind of

used gases.

III. Results and Discussion

From the textural and mechanical stability results summarized in Table I it can be seen that Sample 4, prepared under the highest calcination temperature (950 °C), shows the hardest solid structure. However, its basic texture properties represented by the surface area and porosity were the worst due to the sintering process which took place during the calcination. On the other hand, Sample 1, prepared under the lowest calcination temperature, was unsuitable for hydrogen storage owing to its very low mechanical stability. Samples 2 and 3 have similar texture properties (see Table I and Fig. 2); Sample 3 possesses, however, higher mechanical stability. On account of both textural and mechanical properties, Fe_2O_3/Al_2O_3 (Sample 3, calcined at 850 °C), as well as the reduced form of this pellet (Fe/Al_2O_3), were selected for the chromatographic evaluation of transport characteristics (see Table I). Textural properties of Fe/Al_2O_3 pellets are summarized in Table II.

TABLE II
Textural Properties of Fe/Al_2O_3 Cylindrical Pellets

S_{BET}	V_{mic}	*Total intrusion volume*	ρ_{He}	ρ_{Hg}	ε
[m^2/g]	[mm^3/g]	[cm^3/g]	[g/cm^3]	[g/cm^3]	[–]
20.6	4.7	0.6339	4.037	1.039	0.74

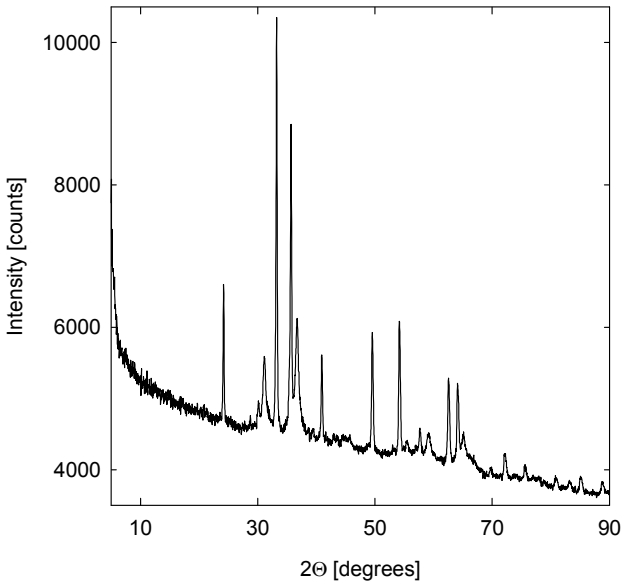

Fig. 5 X-ray diffractograms for Fe_2O_3/Al_2O_3 sample

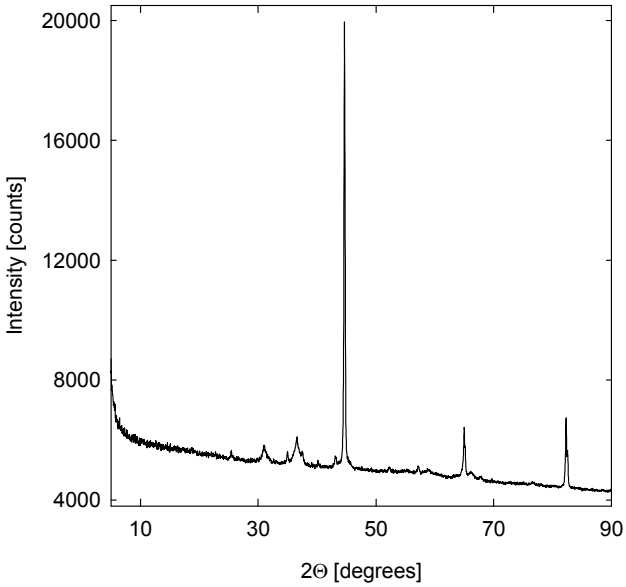

Fig. 6 X-ray diffractograms for Fe/Al_2O_3 sample

Figs. 5 and 6 show XRD diffractograms of Fe_2O_3/Al_2O_3 and Fe/Al_2O_3. Diffraction peaks in Fig. 5 clearly show the presence of the well-defined low dispersed crystalline hematite (Fe_2O_3) with the reflection peaks located at angles 24.2°, 33.2°, 35.7°, 39.4°,40.9°, 49.5°, 54.1° , 64.1°, which correspond to a rhombohedral phase (the highest intensity of reflection appeared in range 33.2–35.7°). In addition to the large amount of the hematite, the presence of the magnetite (Fe_3O_4) in cubic phase (corresponding reflection peaks: 31.2°, 36.7°, 55.5°) as well as orthorhombic phase (corresponding diffraction peaks: 30.1°, 43°, 44.6°) are visible. No distinct diffracting peaks were found for alumina — this indicates an amorphous phase of Al_2O_3. Fe_2O_3/Al_2O_3 sample after reduction (see Fig. 6) clearly shows three groups of peaks on the diffractogram. The reflection peak with the highest intensity (located at angles 44.7°) corresponds to metallic iron (ferrite). In addition, two species based on the mixed (Fe Al) oxides can be considered: hercynite ($FeAl_2O_4$) phase can be seen in the XRD curves with angles 18.8°, 31°, 36.5°, 55.3°, 58.9°. On the other hand, the presence of reflection peaks with the low score located at 25.5°, 35°, 37.5° 43.1°, 52.3°, 57.2°, 66.1° point to the formation of low quantities of $(Al,Fe)_2O_3$ compound during the reduction process. Similarly to the Fe_2O_2/Al_2O_3 sample, the distinct diffraction peaks associated with the pure crystallized Al_2O_3 were not detected.

The parameters of processes in the column (i.e. convection time, t_c, diffusion time, t_{dif}, and Peclet number, Pe) were evaluated from the peak shape. The effective diffusion coefficients of all tracer/carrier gas pairs in columns packed both with pellets Fe_2O_3/Al_2O_3 and Fe/Al_2O_3 were computed from corresponding diffusion times, t_{dif}, obtained by time-domain fitting of column responses. An algorithm of this parameter evaluation can be found elsewhere [19]–[22]. The effective diffusion coefficients include a contribution from the

Knudsen diffusion mechanism and the bulk (molecular) diffusion mechanism according to the Bosanquet formula [23]:

$$\frac{1}{D_{TC}} = \frac{1}{\langle r \rangle \psi K_T} + \frac{1}{\psi \mathsf{D}_{TC}^m} \tag{6}$$

with the binary bulk diffusion coefficients of the pair C–T, D_{TC}^m, and transport parameters $\langle r \rangle \psi$ and ψ [14] ($\langle r \rangle$ is the integral mean transport-pore radius, and ψ is the ratio of transport-pore porosity and tortuosity). K_T is the tracer Knudsen coefficient defined as:

$$K_T = \frac{2}{3}\sqrt{\frac{8R_g T}{\pi M_T}} \tag{7}$$

with the gas constant, R_g, temperature, T, and tracer molecular weight, M_T. Equation (6) can be rearranged into a form, which permits easy graphical solution:

$$t_{dif} K_T = \frac{(d_p/2)^2 \varepsilon}{\langle r \rangle \psi} + \frac{(d_p/2)^2}{\psi} \frac{K_T}{\mathsf{D}_{TC}^m} \tag{8}$$

where d_p denotes the equivalent sphere diameter (diameter of the sphere with the same ratio of outer surface and volume as the pellet); ε is the sample porosity.

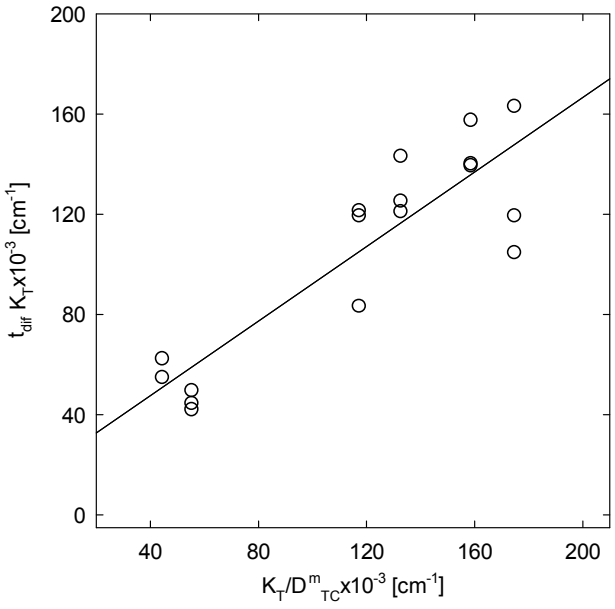

Fig. 7 Diffusion times for Fe_2O_3/ Al_2O_3 (Sample 3) from chromatographic measurements in coordinate $t_{dif} K_T$ versus K_T / D_{TC}^m

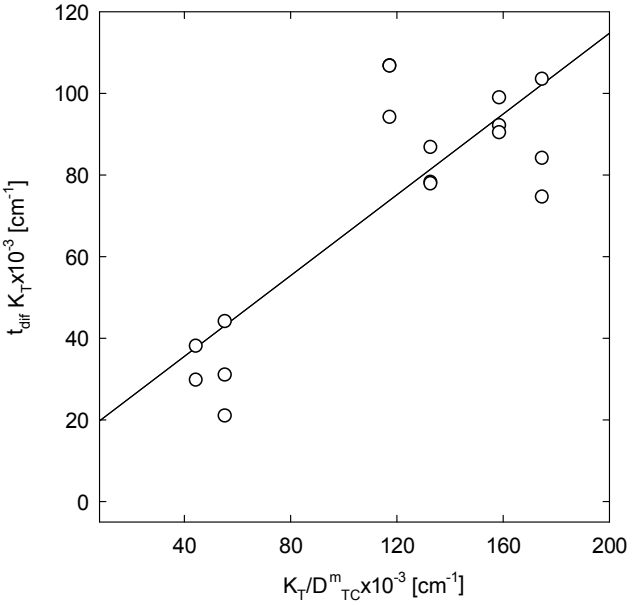

Fig. 8 Diffusion times for Fe/Al_2O_3 (reduced form of Sample 3) from chromatographic measurements in coordinate $t_{dif} K_T$ versus K_T / D_{TC}^m

Transport parameters $\langle r \rangle \psi$ and ψ were evaluated from the slope and intercept of the straight-line $t_{dif} K_T$ versus K_T / D_{TC}^m according to (8) (see Figs. 7 and 8). The obtained transport parameters and the mean transport-pore radii $\langle r \rangle = (\langle r \rangle \psi)/\psi$ are summarized in Table III.

As can be seen (cf. Table III) the mean transport pore radii, $\langle r \rangle$, of both Fe_2O_3/Al_2O_3 and Fe/Al_2O_3 samples are similar (356 nm and 313 nm, respectively), but the parameter ψ, which includes porosity of transport pores, is higher for the metal containing sample (0.090 in comparison with 0.052 for oxidic sample). Thus, Fe/Al_2O_3 pellets have a rather higher porosity of transport pores than Fe_2O_3/Al_2O_3 pellets, which is in agreement with porosity data from the textural analysis (compare Tables I and II). On the other hand, the changes of transport and texture characteristics taking place during the iron oxide reduction (see (1)) are not too high, which is quite significant for the use in the hydrogen storage process (according to the targets defined by the U.S. Department of Energy a viable method for storing hydrogen on board of a vehicle must be able to repeat hydrogen storage cycle at least 500 times [24]).

TABLE III
TRANSPORT PARAMETERS EVALUATED FROM CHROMATOGRAPHIC MEASUREMENTS

Sample	$+r,\psi$ [nm]	ψ [–]	$+r$, [nm]
Fe_2O_3/Al_2O_3	18.5	0.052	355.8
Fe/Al_2O_3	28.2	0.090	313.3

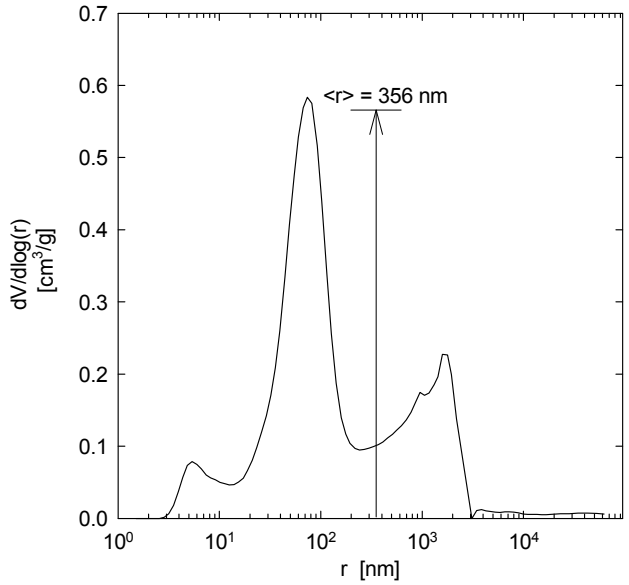

Fig. 9 Comparison of the pore-size distribution curves (from high-pressure mercury porosimetry – solid line) with mean transport-pore radii (from SPSC method) for Fe_2O_3/Al_2O_3 sample

Figs. 9 and 10 compares the mean transport pore radii, $\langle r \rangle$, evaluated from the analysis of chromatographic experiments with the pore-size distribution (PSD) obtained from a high-pressure mercury porosimetry. As can be seen the mean transport pore radii are positioned approximately in the middle between the PSD peaks. It follows, that the gas diffusion transport takes place predominantly through rather wider pores.

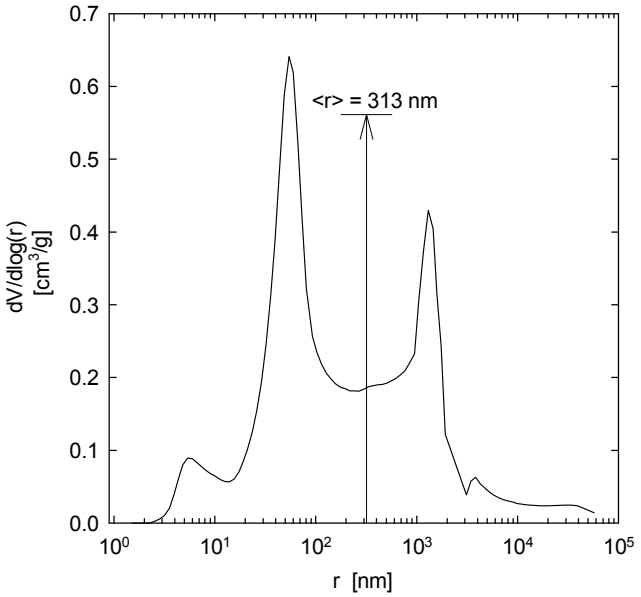

Fig. 10 Comparison of the pore-size distribution curves (from high-pressure mercury porosimetry – solid line) with mean transport-pore radii (from SPSC method) for Fe/Al_2O_3 sample

IV. CONCLUSIONS

Four types of cylindrical pellets consisted from ferric oxide/aluminium oxide powders were prepared under different calcination temperatures. From the textural data it is clearly seen that the influence of calcination temperature on textural properties as well as on the mechanical stability of tablets is very significant—this fact points to the importance of the calcination temperature during the preparation of cylindrical pellets. Sample 4 prepared at the highest calcination temperature (950 ^{o}C) shows the hardest solid structure of all samples. However, this sample was almost without pores due to the sintering process which takes place under these conditions. On the other hand, Sample 1 prepared at 550 ^{o}C exhibited a very soft structure, which limits its use in the hydrogen storage process. Both Samples 2 and 3 possess very similar textural properties but Sample 3 reveals better mechanical stability. Therefore, Sample 3 was chosen as an appropriate testing material for hydrogen storage experiments.

Transport parameters of the Fe_2O_3/Al_2O_3 sample (Sample 3) and the Fe/Al_2O_3 sample obtained by chemical reduction were evaluated by the chromatographic technique in the single pellet-string arrangement. Owing to that, these transport parameters are material constants of porous solids and, hence, independent of the nature of used gases, as well as of temperature and pressure. They can be used for estimation of the effective diffusion coefficients for any tracer/carrier gas pairs. This fact opens the possibility of the direct utilization of the estimated transport characteristics for optimization of porous structure in materials used for hydrogen storage.

REFERENCES

[1] M. Gao, R. B. Gupta, S. Hodoshima, R. Krishnamurthy, K. K. Pant, Y. Saito, S. Satyapal, G. J. Thomas, "Transportation and storage of hydrogen" in *Hydrogen fuel: production, transport, and storage*, R. B. Gupta, Ed. Boca Raton: CRC Press, 2008, pp. 325–474.

[2] P. B. Tarman, D. V. Punwani, "Hydrogen production by the steam-iron process, "*Proc. Intersoc. Energy Convers. Eng. Cont.*, vol. 11, pp. 286–293, 1976.

[3] K. Otsuka, A. Mito, S. Takenaka, I. Yamanaka, "Production of hydrogen from methane without CO_2-emission mediated by indium oxide and iron oxide, " *Int. J. Hydrogen Energy*, vol. 26, pp. 191–194, 2001.

[4] K. Otsuka, T. Kaburagi, C. Yamada, S. Takenaka, "Chemical storage of hydrogen by modified iron oxides," *J. Power Sources*, vol. 122, pp. 111–121, 2003.

[5] K. Otsuka, C. Yamada, T. Kaburagi, S. Takenaka, "Hydrogen storage and production by redox of iron oxide for polymer electrolyte fuel cell vehicles," *Int. J. Hydrogen Energy*, vol. 28, pp. 335–342, 2003.

[6] J. A. Peña, E. Lorente, E. Romero, J. Herguido, "Kinetic study of the redox process for storing hydrogen. Reduction stage," *Catal. Today*, vol. 116, pp. 439–444, 2006.

[7] E. Lorente, J. A. Peña, J. Herguido, "Kinetic study of the redox process for separating and storing hydrogen: Oxidation stage and ageing of solid," *Int. J. Hydrogen Energy*, vol. 33, pp. 615–626, 2008.

[8] K. Svoboda, G. Slowinski, J. Rogut, D. Baxter, "Thermodynamic possibilities and constrains for pure hydrogen production by iron based chemical looping process at lower temperatures," *Energy Convers. Manag.*, vol. 48, pp. 3063–3073, 2007.

[9] S. Takenaka, T. Kaburagi, C. Yamada, K. Nomura, K. Otsuka, "Storage and supply of hydrogen by means of the redox of the iron oxides modified with Mo and Rh species," *J. Catal.*, vol. 228, pp. 66–74, 2004.

[10] S. Takenaka, K. Nomura, N. Hanaizumi, K. Otskuka, "Storage and formation of pure hydrogen mediated by the redox of modified iron oxides," *Appl. Catal. A Gen*., vol. 282, pp. 333–341, 2005.

[11] K. Otsuka, A. Mito, S. Takenaka, I. Yamanaka, "Production of hydrogen from ethane without CO_2-emission mediated by indiumoxide and iron oxide," *Int. J. Hydrogen Energy*, vol. 26, pp. 191–194, 2001.

[12] D. S. Scott, W. Lee, J. Papa, "The measurement of transport coefficients in gas-solid heterogeneous reactions," *Chem. Eng. Sci.*, vol. 29, pp. 2155–2167, 1974.

[13] M. Kubín, "Beitrag zur Theorie der Chromatographie," *Collect. Czech. Chem. Commun*., vol. 30, pp. 1104–1118, 1965.

[14] E. Kučera, "Contribution to the theory of chromatography: linear non-equilibrium elution chromatography," *J. Chromatogr*., vol. 19, pp. 237–248, 1965.

[15] P. Schneider, J. M. Smith, "Adsorption rate constants from chromatography," *AICHE J*., vol. 14, pp. 762–771, 1968.

[16] P. Schneider, "Time-domain expression for impulse response (chromatographic) curve for the Kubín-Kučera model of adsorption column," *Chem. Eng. Sci*., vol. 39, pp. 927–929, 1984.

[17] O. Šolcová, P. Schneider, "Extra column effect in determination of rate parameters by the chromatographic methods," *Collect. Czech. Chem. Commun*., vol. 61, pp. 844–855, 1996.

[18] P. Schneider, "Multicomponent isothermal diffusion and forced flow of gases in capillaries," *Chem. Eng. Sci*., vol. 33, pp. 1311–1319.

[19] T. Starý, O. Šolcová, P. Schneider, M. Marek, "Effective diffusivities and pore-transport characteristics of washcoated ceramic monolith for automotive catalytic converter," *Chem. Eng. Sci.*, vol. 61, pp. 5934–5943, 2006.

[20] O. Šolcová, P. Schneider, "Axial dispersion in single pellet-string columns with non-porous packing," *Chem. Eng. Sci.*, vol. 59, pp. 1301–1307, 2004.

[21] O. Šolcová, K. Soukup, P. Schneider, "Axial dispersion in single-string columns packed with unusually shaped porous pellets," *Chem. Eng. J*., vol. 110, pp. 11–18, 2005.

[22] O. Šolcová, K. Soukup, P. Schneider, "Diffusion coefficients and other transport characteristics of peculiarly shaped porous materials in the single pellet-string column," *Micro. Meso. Mat.*, vol. 91, pp. 100–106, 2006.

[23] O. Šolcová, P. Schneider, "Transport characteristics of porous solids derived from chromatographic measurements," *Stud. Surf. Sci. Catal*., vol. 144, pp. 475–482, 2002.

[24] U.S. Department of Energy. (2006, March). FreedomCAR and fuel partnership plan. Available: http://www1.eere.energy.gov/vehiclesandfuels/pdfs/program/fc_fuel_partnership_plan.pdf